

# A non-local model for the description of twinning in polycrystalline materials at moderate strains: application to a magnesium alloy

 Charles Mareau<sup>1</sup> and  Hamidreza Abdolvand<sup>2</sup>

<sup>1</sup> Arts et Metiers Institute of Technology, LAMPA, HESAM Université, F-49035 Angers, France

<sup>2</sup> Department of Mechanical and Materials Engineering, Western University, London, Ontario, N6A 5B9, Canada

A polycrystalline plasticity model, which incorporates the contribution of deformation twinning, is proposed. For this purpose, each material point is treated as a composite material consisting of a parent constituent and multiple twin variants. In the constitutive equations, the twin volume fractions and their spatial gradients are treated as external state variables to account for the contribution of twin boundaries to free energy. The set of constitutive relations is implemented in a spectral solver, which allows solving the differential equations resulting from equilibrium and compatibility conditions. The proposed model is then used to investigate the behavior of a AZ31 magnesium alloy. For the investigated loading conditions, the mechanical behavior is controlled by the joint contribution of basal slip and tensile twinning. Also, according to the numerical results, the development of crystallographic texture, morphological texture and internal stresses is consistent with the experimental observations of the literature.

**Keywords** microstructures, twinning, constitutive behaviour, crystal plasticity, spectral method

## 1 Introduction

For metallic alloys with a hexagonal close packed (hcp) structure, the mechanical behavior is impacted by the competition between deformation twinning and crystallographic slip. Indeed, for such materials, plastic deformation is partly accommodated by mechanical twinning because of the limited number of easy slip systems.

In contrast with crystallographic slip, which is a rather progressive deformation mechanism, twinning results in significant and rapid microstructural transformations, even at moderate strains. For instance, many experimental studies have shown that, depending on loading conditions, texture development is affected by twinning in the early stages of deformation (Brown et al. 2005; Jiang et al. 2007; Xu, Holt, and Daymond 2009). Also, due to the resistance opposed by surrounding grains, the growth of deformation twins is associated with the development of an internal stress field. Neutron diffraction techniques have allowed investigating the evolution of this internal stress field through the evaluation of the resulting lattice strains. Such techniques have been used to study load partition between twin and parent grains in magnesium (Wu et al. 2008; Clausen et al. 2008) and zirconium (Xu, Holt, Daymond, et al. 2008) alloys. In the recent years, some alternative techniques with a higher spatial resolution have been used to evaluate internal stresses. For instance, Arul Kumar et al. (2018) used micro-Laue X-ray diffraction techniques to estimate the stress state in the vicinity of a twin in magnesium. They concluded that the formation of a twin divides the parent grain into two non-interacting domains. Nervo et al. (2016) used diffraction contrast tomography to investigate the twinning behavior of a titanium alloy. Their results suggest that prismatic  $\langle a \rangle$  slip favors the formation and clustering of twins. Twin variant selection in titanium has been studied with high resolution electron backscatter diffraction techniques by Guo et al. (2017). They found that variant selection is controlled by the local stress state. Three dimensional X-ray diffraction (3D-XRD) techniques (Poulsen et al. 2001) have allowed measuring the positions, orientations, volume fractions and elastic strains of multiple grains during the *in-situ* deformation of a magnesium alloy (Aydiner et al. 2009; Abdolvand, Majkut, et al. 2015). The corresponding dataset has been used to identify twin-parent pairs and evaluate the grain volume-averaged stress tensors. For a given twin-parent pair, Aydiner et al. (2009) and Abdolvand, Majkut, et al. (2015) found that the average normal stress acting on the habit plane is almost the same for the twin and parent grains. However, for a twin grain, the average tangential stress acting on the twin habit plane along the twin direction is lower than that of the corresponding parent grain.

Different strategies have been explored to include the contribution of twinning in the context of polycrystalline plasticity. Mean-field polycrystalline models have been widely used with either rate-independent (Agnew et al. 2006; Xu, Holt, and Daymond 2008; Clausen et al. 2008) or rate-dependent (Proust, Tomé, and Kaschner 2007; Mareau et al. 2011; Wang et al. 2018) crystal plasticity-based constitutive models. Though some solutions have been proposed (Cherkaoui 2003; Juan et al. 2014), the interactions between parent grains and twin domains are generally evaluated only in an averaged manner with the

mentioned approaches. Also, by definition, mean-field polycrystalline models ignore the role of intragranular stresses on the deformation behavior. Full-field polycrystalline models rely on either the finite element method (Kalidindi 2001; Abdolvand, Daymond, et al. 2011; Staroselsky et al. 2003; Chang et al. 2015; Cheng et al. 2015; Ardeljan, Beyerlein, et al. 2016; Paramatmuni and Dunne 2020) or the spectral method (Mareau et al. 2016; Paramatmuni and Kanjarla 2019) to evaluate the intragranular stress and strain gradients resulting from twinning. Since the associated constitutive models often use a pseudo-slip formulation, the morphological texture evolution resulting from the formation of twins is not always considered. To circumvent these limitations, some procedures have been proposed to insert twinned domains in a polycrystalline microstructure (Ardeljan, McCabe, et al. 2015; Cheng et al. 2017). However, such procedures require an *a priori* knowledge of the twin morphology and ignore the contribution of interfacial energy. The phase-field method provides a convenient thermodynamic framework to consider the increase of surface energy resulting from the formation of twin boundaries (Clayton et al. 2011; Kondo et al. 2014; Liu et al. 2018; Grilli et al. 2020). In the context of twinning, the phase-field method treats the twin volume fraction and its spatial gradient as state variables, which allows tracking twin boundaries without any complex numerical procedure.

In the present work, a non-local constitutive model, which incorporates the contribution of twinning to plastic deformation, is proposed. Constitutive relations are developed in the context of crystal plasticity. Also, the proposed model is non-local in the sense that the spatial gradients of the twin volume fractions are included in the list of state variables, which allows considering the contribution of twin boundaries to free energy. The present paper is organized as follows. The constitutive equations are provided in the first part of this paper. In the second part, the proposed model is used to investigate the impact of deformation twinning on the behavior of a AZ31 magnesium alloy. The numerical results allow discussing several aspects of deformation twinning, including twin variant selection, texture development and internal stress evolution.

## 2 Model description

### 2.1 Composite material assumption

As illustrated by Figure 1, the present approach treats each material point as a composite material to deal with the growth of twinned domains within a polycrystalline volume element. Each material point thus consists of  $n + 1$  constituents: one parent constituent (with volume fraction  $\phi_m$ ) and  $n$  child constituents (with volume fractions  $\phi_{c=1,n}$ ), which correspond to the  $n$  twin variants. For any material point, the volume fractions should satisfy the following condition:

$$\sum_c \phi_c + \phi_m = 1. \quad (1)$$

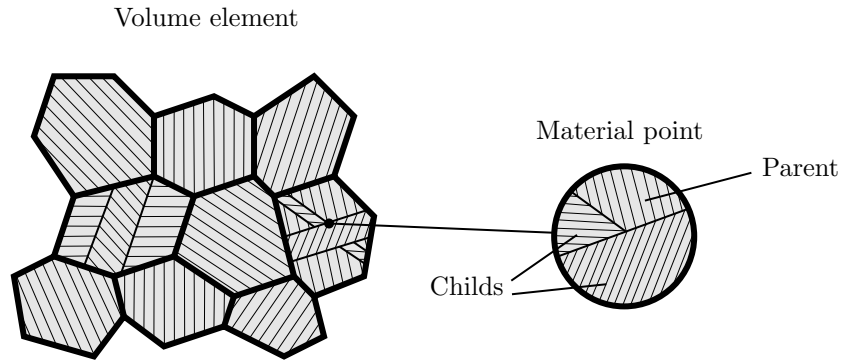


**Figure 1:** Each material point is treated as a composite material consisting of a parent constituent and multiple child constituents corresponding to the different twin variants.

According to the averaging relations of homogenization theory, the total strain and stress tensors ( $\epsilon$  and  $\sigma$ ) are given by:

$$\epsilon = \sum_c \phi_c \epsilon_c + \phi_m \epsilon_m, \quad (2)$$

$$\sigma = \sum_c \phi_c \sigma_c + \phi_m \sigma_m. \quad (3)$$

In the following, the stress state is assumed to be uniform within the different constituents during a deformation process, that is:

$$\sigma_c = \sigma_m = \sigma. \quad (4)$$

As a result of the composite material assumption, deformation twinning is treated as a progressive process. Indeed, a material point can be either fully untwinned (i.e.  $\phi_m = 1$ ), fully twinned (i.e.  $\phi_m = 0$ ) or in an intermediate situation (i.e.  $0 < \phi_m < 1$ ). Also, while the stress state is uniform within the different constituents of a material point, the stress state is not identical for the parent and twinned domains of a given grain.

## 2.2 Equilibrium equations

The development of the constitutive model for twinning relies on the introduction of an extended set of state variables. In contrast with the classical theory, which uses the infinitesimal strain tensor  $\boldsymbol{\varepsilon}$  as the sole external state variable<sup>1</sup>, the volume fractions  $\phi_c$  associated with the different twin variants and the corresponding spatial gradients  $\nabla\phi_c$  are also treated as external state variables. The consequence is that the power developed by internal forces includes the contributions resulting from the evolutions of the strain field and twin volume fractions. Specifically, the density of power developed by internal forces  $p_i$  is given by (Nguyen 2015):

$$p_i = \boldsymbol{\sigma} : \dot{\boldsymbol{\varepsilon}} + \sum_c \xi_c \dot{\phi}_c + \sum_c \boldsymbol{\eta}_c \cdot \nabla \dot{\phi}_c, \quad (5)$$

where  $\boldsymbol{\sigma}$  is the Cauchy stress tensor,  $\xi_c$  is the scalar microstress power-conjugate to the volume fraction rate  $\dot{\phi}_c$  and  $\boldsymbol{\eta}_c$  is the vector microstress power-conjugate to the spatial gradient  $\nabla\dot{\phi}_c$ .

The evolution of the strain field and twin volume fractions is governed by some equilibrium equations, which can be derived from the application of an extended principle of virtual power (see Frémond et al. (1996) in the context of damage or Cermelli et al. (2002) in the context of crystal plasticity). The direct consequence of this assumption is that the classical equilibrium equations of continuum mechanics are supplemented with some additional equilibrium equations<sup>2</sup>:

$$\boldsymbol{\sigma} \cdot \nabla = \mathbf{0} \text{ and } \boldsymbol{\sigma} = \boldsymbol{\sigma}^T, \quad (6)$$

$$\xi_c - \nabla \cdot \boldsymbol{\eta}_c = 0, \quad \forall c. \quad (7)$$

In the literature, the later equation is often referred to as the microforce balance equation (Cermelli et al. 2002).

## 2.3 State equations

For a material point, the free energy density  $a$  is decomposed according to:

$$a = \sum_c \phi_c a_c + \phi_m a_m + \sum_c \gamma_{c/m}, \quad (8)$$

where  $a_m$  and  $a_c$  are the bulk contributions of parent and child constituents while  $\gamma_{c/m}$  is the surface contribution associated with a parent/twin interface. For the construction of constitutive relations, the total strain tensor is decomposed into elastic (superscript  $e$ ), plastic (superscript  $p$ ) and transformation (superscript  $tw$ ) contributions. In the context of infinitesimal transformations, one obtains:

$$\boldsymbol{\varepsilon}_c = \boldsymbol{\varepsilon}_c^e + \boldsymbol{\varepsilon}_c^p + \boldsymbol{\varepsilon}_c^{tw}, \quad (9)$$

$$\boldsymbol{\varepsilon}_m = \boldsymbol{\varepsilon}_m^e + \boldsymbol{\varepsilon}_m^p. \quad (10)$$

It is worth mentioning that, for a child constituent, the transformation strain is calculated from the characteristic shear strain  $\gamma^{tw}$ , which is constant, with:

$$\boldsymbol{\varepsilon}_c^{tw} = \text{sym}(\boldsymbol{t}_c^\alpha \otimes \boldsymbol{k}_c^\alpha) \gamma^{tw}, \quad (11)$$

where  $\boldsymbol{t}_c$  is the twinning direction and  $\boldsymbol{k}_c$  is the twin plane normal associated to the corresponding twinning system. Also, within the framework of crystal plasticity, the plastic strain tensors are given by:

$$\boldsymbol{\varepsilon}_c^p = \sum_\alpha \text{sym}(\boldsymbol{m}_c^\alpha \otimes \boldsymbol{n}_c^\alpha) \gamma_c^\alpha, \quad (12)$$

$$\boldsymbol{\varepsilon}_m^p = \sum_\alpha \text{sym}(\boldsymbol{m}_m^\alpha \otimes \boldsymbol{n}_m^\alpha) \gamma_m^\alpha, \quad (13)$$

where  $\boldsymbol{m}^\alpha$ ,  $\boldsymbol{n}^\alpha$  and  $\gamma^\alpha$  are respectively the slip direction, the slip plane normal and the plastic shear strain of the  $\alpha$ th slip system for either the parent or child constituents (subscript  $m$  or  $c$ ).

<sup>1</sup> In a thermomechanical context, one would treat temperature as an additional external state variable.

<sup>2</sup> For simplicity, the contributions of volume forces and inertia effects are excluded.

In the following, the bulk contributions to free energy are defined as follows:

$$a_c = \frac{1}{2} \boldsymbol{\varepsilon}_c^e : \mathbb{C}_c : \boldsymbol{\varepsilon}_c^e + \frac{1}{2} \sum_{\alpha} \varrho_c^{\alpha} \sum_{\beta} H^{\alpha\beta} \varrho_c^{\beta}, \quad (14)$$

$$a_m = \frac{1}{2} \boldsymbol{\varepsilon}_m^e : \mathbb{C}_m : \boldsymbol{\varepsilon}_m^e + \frac{1}{2} \sum_{\alpha} \varrho_m^{\alpha} \sum_{\beta} H^{\alpha\beta} \varrho_m^{\beta}. \quad (15)$$

In the above equations, the first term represents the elastic strain energy while the second term corresponds to defect energy. The stiffness tensors associated with the parent or child constituents are denoted by  $\mathbb{C}_m$  and  $\mathbb{C}_c$ . Also,  $\varrho_m^{\alpha}$  and  $\varrho_c^{\alpha}$  are the isotropic hardening variables associated with the  $\alpha$ th slip system. The possible interactions between different slip systems are described with the matrix  $H$ .

For the interfacial energy, the suggestion of Liu et al. (2018), which includes both local and non-local contributions, is adopted:

$$\gamma_{c/m} = \frac{1}{2} \nabla \phi_c \cdot \mathbf{K}_c \cdot \nabla \phi_c + A \phi_c (1 - \phi_c). \quad (16)$$

The local contribution is minimum for either  $\phi_c = 0$  or  $\phi_c = 1$ , which correspond to the equilibrium states of a fully untwinned or fully twinned material point. A simple choice for  $\mathbf{K}_c$  consists in writing:

$$\mathbf{K}_c = B \mathbf{k}_c \otimes \mathbf{k}_c + C (1 - \mathbf{k}_c \otimes \mathbf{k}_c). \quad (17)$$

The anisotropic gradient contribution allows considering the fact that the interfacial energy along the twin boundary is smaller than that of the twin tip. The surface energy associated with the twin/parent interfaces, as well as the width of the twin/parent interfaces, is controlled by the  $A$ ,  $B$  and  $C$  material parameters.

For the development of constitutive relations, it is convenient to define the thermodynamic forces associated with the different state variables. First, when no viscous contribution to the stress state is considered, the stress tensors  $\boldsymbol{\sigma}_c$  and  $\boldsymbol{\sigma}_m$  are obtained from:

$$\boldsymbol{\sigma}_c = \frac{\partial a_c}{\partial \boldsymbol{\varepsilon}_c} = \mathbb{C}_c : \boldsymbol{\varepsilon}_c^e, \quad (18)$$

$$\boldsymbol{\sigma}_m = \frac{\partial a_m}{\partial \boldsymbol{\varepsilon}_m} = \mathbb{C}_m : \boldsymbol{\varepsilon}_m^e. \quad (19)$$

In a similar fashion, if the microstress vector  $\boldsymbol{\eta}_c$  has a purely energetic origin (*i.e.* it does not depend on  $\nabla \dot{\phi}_c$ ), the corresponding state equation is:

$$\boldsymbol{\eta}_c = \frac{\partial a}{\partial \nabla \phi_c} = \mathbf{K}_c \cdot \nabla \phi_c. \quad (20)$$

The resolved shear stresses  $\tau_c^{\alpha}$  and  $\tau_m^{\alpha}$ , which act on the different slip systems, are evaluated from the projections of the corresponding stress tensors:

$$\tau_c^{\alpha} = -\frac{\partial a_c}{\partial \gamma_c^{\alpha}} = \mathbf{m}_c^{\alpha} \cdot \boldsymbol{\sigma}_c \cdot \mathbf{n}_c^{\alpha}, \quad (21)$$

$$\tau_m^{\alpha} = -\frac{\partial a_m}{\partial \gamma_m^{\alpha}} = \mathbf{m}_m^{\alpha} \cdot \boldsymbol{\sigma}_m \cdot \mathbf{n}_m^{\alpha}. \quad (22)$$

The critical resolved shear stresses (CRSS)  $r_c^{\alpha}$  and  $r_m^{\alpha}$  are connected to the corresponding isotropic hardening variables according to:

$$r_c^{\alpha} = \frac{\partial a_c}{\partial \varrho_c^{\alpha}} = \sum_{\beta} H^{\alpha\beta} \varrho_c^{\beta}, \quad (23)$$

$$r_m^{\alpha} = \frac{\partial a_m}{\partial \varrho_m^{\alpha}} = \sum_{\beta} H^{\alpha\beta} \varrho_m^{\beta}. \quad (24)$$

Finally, the thermodynamic force associated with the twin volume fraction  $\phi_c$ , which is denoted by  $\zeta_c$ , is given by:

$$\zeta_c = \frac{\partial a}{\partial \phi_c} = (a_c - a_m) + A (1 - 2\phi_c). \quad (25)$$

## 2.4 Evolution equations

In a purely mechanical context, the density of power being dissipated into heat  $d$  is obtained from the difference between the power developed by internal forces and the evolution rate for free energy:

$$d = p_i - \dot{a}. \quad (26)$$

Using the definitions of the thermodynamic forces, the evolution rate for the specific free energy is given by:

$$\begin{aligned} \dot{a} = & \sum_c \phi_c \left( \boldsymbol{\sigma}_c : \dot{\boldsymbol{\varepsilon}}_c - \sum_\alpha (\tau_c^\alpha \dot{\gamma}_c^\alpha - r_c^\alpha \dot{\varrho}_c^\alpha) \right) + \phi_m \left( \boldsymbol{\sigma}_m : \dot{\boldsymbol{\varepsilon}}_m - \sum_\alpha (\tau_m^\alpha \dot{\gamma}_m^\alpha - r_m^\alpha \dot{\varrho}_m^\alpha) \right) \\ & + \sum_c \left( \xi_c \dot{\phi}_c + \boldsymbol{\eta}_c \cdot \nabla \dot{\phi}_c \right). \end{aligned} \quad (27)$$

Also, the composite material assumption allows reformulating the density of power developed by internal forces, which is given by Equation (5), as follows:

$$p_i = \sum_c \phi_c \boldsymbol{\sigma}_c : \dot{\boldsymbol{\varepsilon}}_c + \phi_m \boldsymbol{\sigma}_m : \dot{\boldsymbol{\varepsilon}}_m + \sum_c \dot{\phi}_c \boldsymbol{\sigma} : (\boldsymbol{\varepsilon}_c - \boldsymbol{\varepsilon}_m) + \sum_c \xi_c \dot{\phi}_c + \sum_c \boldsymbol{\eta}_c \cdot \nabla \dot{\phi}_c. \quad (28)$$

According to the above expression, the power developed by internal forces is spent to deform the individual constituents and to expand/contract twinned domains. Combining (27) and (28), the expression of the dissipation source becomes:

$$d = \sum_c \phi_c \left( \sum_\alpha (\tau_c^\alpha \dot{\gamma}_c^\alpha - r_c^\alpha \dot{\varrho}_c^\alpha) \right) + \phi_m \left( \sum_\alpha (\tau_m^\alpha \dot{\gamma}_m^\alpha - r_m^\alpha \dot{\varrho}_m^\alpha) \right) + \sum_c (\pi_c \dot{\phi}_c). \quad (29)$$

In the above expression, the dissipative force  $\pi_c$ , which governs the evolution of the twin volume fraction, has been introduced:

$$\pi_c = \xi_c - \zeta_c + \boldsymbol{\sigma} : (\boldsymbol{\varepsilon}_c - \boldsymbol{\varepsilon}_m). \quad (30)$$

Combining the equilibrium equation (7) and the state equations (25) and (20) leads to the complete expression of the dissipative force  $\pi_c$ :

$$\pi_c = \nabla \cdot (\mathbf{K}_c \cdot \nabla \phi_c) - A(1 - 2\phi_c) + (a_m - a_c) + \boldsymbol{\sigma} : (\boldsymbol{\varepsilon}_c - \boldsymbol{\varepsilon}_m). \quad (31)$$

According to the above expression, the dissipative force driving the evolution of the twin volume fraction depends not only on the current stress state, but also on the free energy difference between the parent and child constituents and the twin volume fraction in the neighborhood of the material point of interest. This aspect is consistent with the results of Paramatmuni, Guo, et al. (2021), who observed that twin nucleation is governed by the stored energy density. Also, the material parameter  $A$  can be interpreted as a barrier to the initiation of deformation twinning.

In the context of standard materials (Nguyen 2000), the evolution equations, which connect the flux variables to the dissipative forces, are obtained from a dissipation potential  $\varphi$ . For the proposed model, the dissipation potential is decomposed according to:

$$\varphi = \sum_c \phi_c \varphi_c + \phi_m \varphi_m + \sum_c \kappa_{c/m}. \quad (32)$$

The contributions  $\varphi_c$  and  $\varphi_m$  of the child and parent constituents to the dissipation potential are given by:

$$\varphi_c = \sum_\alpha \frac{K}{N+1} \left( \frac{|\tau_c^\alpha| - r_c^\alpha}{K} \right)^{N+1}, \quad (33)$$

$$\varphi_m = \sum_\alpha \frac{K}{N+1} \left( \frac{|\tau_m^\alpha| - r_m^\alpha}{K} \right)^{N+1}. \quad (34)$$

In the above equations,  $K$  and  $N$  are viscosity parameters, which control the resistance to plastic flow and the strain-rate sensitivity. Also, for the contribution of twinning to the dissipation potential, the following choice is adopted:

$$\kappa_{c/m} = \phi_m \frac{L}{M+1} \left( \frac{\langle \pi_c \rangle}{\gamma^{tw} L} \right)^{M+1} + \phi_c \frac{L}{M+1} \left( \frac{\langle -\pi_c \rangle}{\gamma^{tw} L} \right)^{M+1}, \quad (35)$$

where  $L$  and  $M$  are viscosity parameters whose role resembles that of  $K$  and  $N$ . It is emphasized that the contribution of both twinning and detwinning to the dissipation potential have been included in the above expression.

The evolution equations for the different flux variables can be obtained from the differentiation of the dissipation potential with respect to the corresponding dissipative forces. Specifically, the shear strain rates associated with the different slip systems are given by:

$$\dot{\gamma}_c^\alpha = \frac{\partial \varphi_c}{\partial \tau_c^\alpha} = \left( \frac{\langle |\tau_c^\alpha| - r_c^\alpha \rangle}{K} \right)^N \text{sign}(\tau_c^\alpha), \quad (36)$$

$$\dot{\gamma}_m^\alpha = \frac{\partial \varphi_m}{\partial \tau_m^\alpha} = \left( \frac{\langle |\tau_m^\alpha| - r_m^\alpha \rangle}{K} \right)^N \text{sign}(\tau_m^\alpha). \quad (37)$$

The evolution of the isotropic hardening variables is controlled by:

$$\dot{\rho}_c^\alpha = -\frac{\partial \varphi_c}{\partial r_c^\alpha} = \left( \frac{\langle |\tau_c^\alpha| - r_c^\alpha \rangle}{K} \right)^N = |\dot{\gamma}_c^\alpha|, \quad (38)$$

$$\dot{\rho}_m^\alpha = -\frac{\partial \varphi_m}{\partial r_m^\alpha} = \left( \frac{\langle |\tau_m^\alpha| - r_m^\alpha \rangle}{K} \right)^N = |\dot{\gamma}_m^\alpha|. \quad (39)$$

Finally, the evolution equation for the twin volume fraction associated with the  $c$ th twin variant is:

$$\dot{\phi}_c = \frac{\partial \varphi}{\partial \pi_c} = \frac{\phi_m}{\gamma^{tw}} \left( \frac{\langle \pi_c \rangle}{\gamma^{tw} L} \right)^M - \frac{\phi_c}{\gamma^{tw}} \left( \frac{\langle -\pi_c \rangle}{\gamma^{tw} L} \right)^M. \quad (40)$$

It is worth mentioning that the twin volume fraction is not allowed to increase (respectively decrease) when the material point is fully twinned (respectively fully detwinned).

### 3 Application to a AZ31 magnesium alloy

In this section, the proposed model is used to investigate the impact of deformation twinning on the behavior of a AZ31 magnesium alloy, for which some experimental results have been recently obtained by Louca et al. (2021). Specifically, Louca et al. (2021) have extracted some specimens from a rolled AZ31 magnesium plate. The specimens have been annealed to obtain an equiaxed microstructure, with an average grain size of  $50 \mu\text{m}$ . Three-dimensional synchrotron X-ray diffraction techniques (Poulsen et al. 2001) have then been used to determine the position, volume, crystallographic orientation and elastic strains of individual grains during the *in situ* deformation of the polycrystalline AZ31 magnesium alloy. Based on these results, the twin-parent pairs have been identified and the corresponding stress tensors have been evaluated.

For the application of the present model, the field equations resulting from equilibrium and compatibility conditions are solved numerically with the spectral method (Moulinec et al. 1998; Eisenlohr et al. 2013). As shown by Equation (31), the dissipative force driving the evolution of the twin volume fraction involves the divergence of the microstress vector. In the present work, the finite difference method is used for the evaluation of the non-local contribution  $\nabla \cdot (K_c \cdot \nabla \phi_c)$  to this dissipative force.

#### 3.1 Microstructure generation

The volume element used for the application of the spectral method has been obtained from a weighted Voronoi tessellation with fifty seeds. For each seed, the position and weight are respectively given by the center-of-mass and the cube root of the volume of the corresponding grain. The resulting volume element, which is shown in Figure 2, has been discretized into  $128^3$  voxels for the application of the spectral method. Due to the rolling process, most grains have their  $c$ -axis aligned with the normal direction of the plate.

#### 3.2 Loading conditions

In the present work, two different loading paths have been selected to reproduce the experiment of Louca et al. (2021). The first loading path corresponds to a uniaxial compression test along the rolling direction with an axial strain rate of  $5.5 \times 10^{-5} \text{ s}^{-1}$  up to an axial strain of  $-0.50\%$ . The second loading path, which uses the same strain rate, corresponds to a Bauschinger test. A uniaxial compression test is first carried out along the rolling direction up to an axial strain of  $-0.31\%$ . The volume element is then unloaded and finally deformed under uniaxial tension up to an axial strain of  $0.13\%$ .

#### 3.3 Material parameters

The material parameters used to model the mechanical behavior of the AZ31 magnesium alloy are listed in Table 1. The single crystal elastic constants have been taken from the work of Simmons et al. (1971).



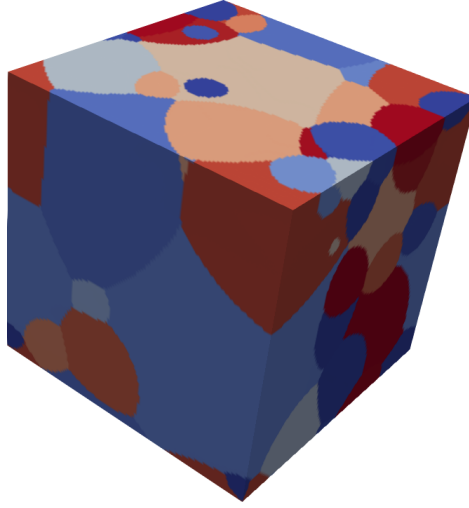


**Figure 2:** Numerical microstructure used for the application of the spectral method. Each color corresponds to a grain.

Four plastic deformation modes are considered: basal (Bas), first order prismatic (Pri) and second order pyramidal (Pyr) slip systems and tensile twinning (TTw). The initial values for the CRSS associated with the different deformation modes and the hardening parameters have been adjusted to reproduce the macroscopic stress-strain behavior under uniaxial compression (see Figures 3 and 9). For simplicity, no distinction is made between latent and self-hardening (i.e.  $H^{\alpha\beta} = H^{\alpha\alpha}$ ). It is worth mentioning that the ratios between the CRSS of the different slip modes correspond to those given by Clausen et al. (2008):  $r_{Pri}/r_{Bas} = 5$ ,  $r_{Pyr}/r_{Bas} = 8.3$ ,  $r_{TTw}/r_{Bas} = 5^3$ . The parameter  $B$  has been selected to obtain a twin boundary energy  $g^{tw}$  of  $0.13 \text{ J/m}^2$  (Pei et al. 2017).

Elasticity				
$\mathbb{C}_{11}$	$\mathbb{C}_{33}$	$\mathbb{C}_{12}$	$\mathbb{C}_{13}$	$\mathbb{C}_{44}$
59.8 GPa	61.7 GPa	23.2 GPa	21.7 GPa	16.4 GPa
Crystallographic slip				
$K$	$N$	$r_{Bas}$	$r_{Pri}$	$r_{Pyr}$
2.0 MPa	20	5.6 MPa	28.0 MPa	46.7 MPa
Twinning				
$L$	$M$	$A$	$B$	$C$
2.0 MPa	20	3.6 MPa	$1.5 \times 10^{-8} \text{ N}$	$1.5 \times 10^{-7} \text{ N}$
Hardening				
$H^{\alpha\beta}$				
1000 MPa				

**Table 1:** Material parameters used for the numerical simulation of the AZ31 magnesium alloy

### 3.4 Results and discussion

#### 3.4.1 Uniaxial compression

The experimental and numerical stress-strain curves obtained under uniaxial compression are plotted in Figure 3. The relative activities<sup>4</sup> of the different slip and twinning deformation modes are also presented. Basal slip systems are first activated (around  $-16 \text{ MPa}$ ), which corresponds to the initial yielding. The activation of twinning systems (around  $-41 \text{ MPa}$ ) and prismatic slip systems (around  $-43 \text{ MPa}$ ) coincides with the transition to the plastic regime. Pyramidal slip systems are never activated during the deformation process.

The local twin volume fraction, which is given by  $1 - \phi_m$ , is plotted in Figure 4. Though the prescribed strain is rather small, twinned domains can clearly be identified at the end of the compression test. The strong morphological texture evolution due to twinning is therefore correctly reproduced. It is worth mentioning that the proposed model does not require any rule to define how nucleation and propagation

<sup>3</sup> Though the CRSS for twinning  $r_{TTw}$  does not appear explicitly in the description of the constitutive model, it is actually given by the ratio  $A/\gamma^{tw}$ .

<sup>4</sup> The relative activity of a deformation mode is defined as its relative contribution to the volume averaged plastic strain tensor.

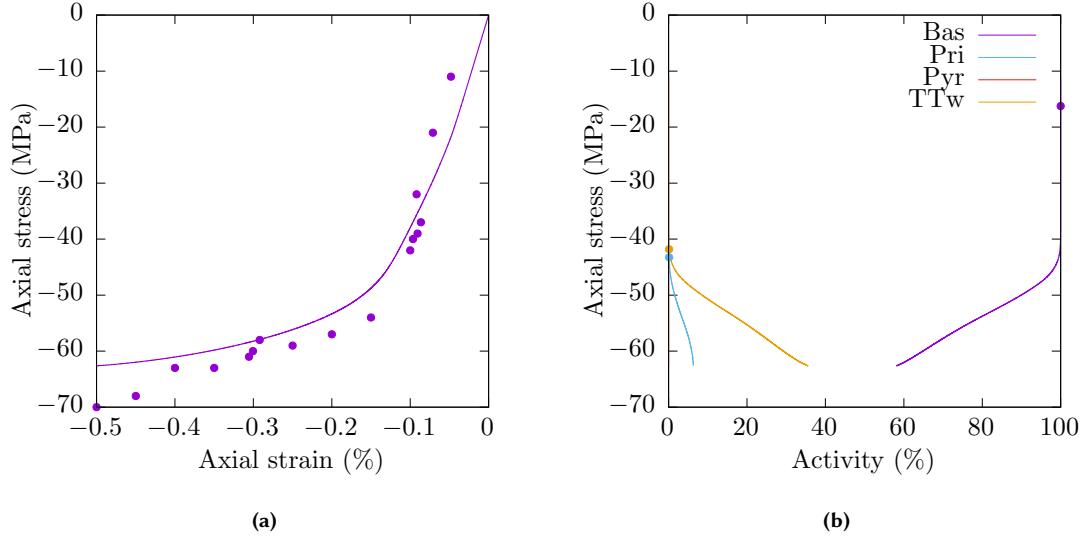


**Figure 3:** (a) Experimental and numerical stress-strain curves obtained for a uniaxial compression test along the rolling direction. (b) Relative activities of the different inelastic deformation modes. The first activation of a given type of slip or twinning system is represented with a dot.

take place. The formation of twinned domains is the direct consequence of the application of equilibrium, compatibility and constitutive equations.

Due to twin variant selection, most twins are oriented with an angle of approximately  $\pm 45^\circ$  with respect to the loading direction. To further investigate how twin variant selection takes place, the twin volume fraction of each variant is plotted as a function of the Schmid factor in Figure 5. Two different options are explored for the evaluation of the Schmid factor. The global Schmid factor is calculated for each twin variant from the orientation of the corresponding system. This factor provides some information regarding the orientation of a twinning system with respect to the macroscopic stress state. The local Schmid factor is evaluated for each twin variant from the grain-averaged stress tensor of the corresponding parent grain. It therefore considers the impact of the intergranular internal stresses resulting from inhomogeneous plastic deformation. Immediately after yielding (i.e. -0.16%), no matter how the Schmid factor is evaluated, the twin volume fraction is generally higher for favorably oriented twin variants. At the end of the compression test (i.e. -0.5%), the maximal twin volume fraction is obtained for some grains for which the local Schmid factor is not maximal, which is a consequence of the local stress relaxation resulting from deformation twinning. Also, as expected, the activity of a twinning system is better represented with the local Schmid factor than the global Schmid factor. Indeed, for a given twin volume fraction, very different values of the global Schmid factor are obtained. For the local Schmid factor, which includes the effect of internal stresses, the range of values for a given twin volume fraction is generally smaller.

As illustrated by Figure 4, important intragranular internal stresses are produced as a result of twinning. Figure 6 shows the evolution of the equivalent von Mises stress within a twinned grain. According to the numerical results, important fluctuations of the stress field within a twinned grain are observed. Specifically, while local stress maxima are obtained near twin boundaries, local stress minima are located close to the center of twinned domains. The later result suggests that stress relaxation occurs within twins.

In the recent years, 3D XRD techniques have been used to investigate the evolution of internal stresses within twinned grains. For a given twin-parent pair, these techniques provide some estimates of the average stress tensors  $\bar{\sigma}^m$  and  $\bar{\sigma}^c$  of the corresponding parent and child grains. For the investigation of internal stresses, it is convenient to introduce the following stress quantities:

$$\bar{\sigma}^m = \mathbf{k}_c \cdot \bar{\sigma}^m \cdot \mathbf{k}_c \text{ and } \bar{\sigma}^c = \mathbf{k}_c \cdot \bar{\sigma}^c \cdot \mathbf{k}_c, \quad (41)$$

$$\bar{\tau}^m = \mathbf{t}_c \cdot \bar{\sigma}^m \cdot \mathbf{k}_c \text{ and } \bar{\tau}^c = \mathbf{t}_c \cdot \bar{\sigma}^c \cdot \mathbf{k}_c. \quad (42)$$

In the above equations,  $\bar{\sigma}^m$  (respectively  $\bar{\sigma}^c$ ) is the average normal stress exerted by the parent (respectively child) grain on the twin habit plane. In a similar fashion,  $\bar{\tau}^m$  (respectively  $\bar{\tau}^c$ ) is the average tangential stress exerted by the parent (respectively child) grain on the twin habit plane along the twinning direction.

For each twin-parent pair, the average normal stress  $\bar{\sigma}^c$  in the twin is plotted as a function of that of the corresponding parent grain  $\bar{\sigma}^m$  in Figure 7. The numerical results are in agreement with the experimental results from the literature (Abdolvand, Majkut, et al. 2015; Louca et al. 2021) showing that, for each pair, the average normal stresses within twins and parents are close to each other.



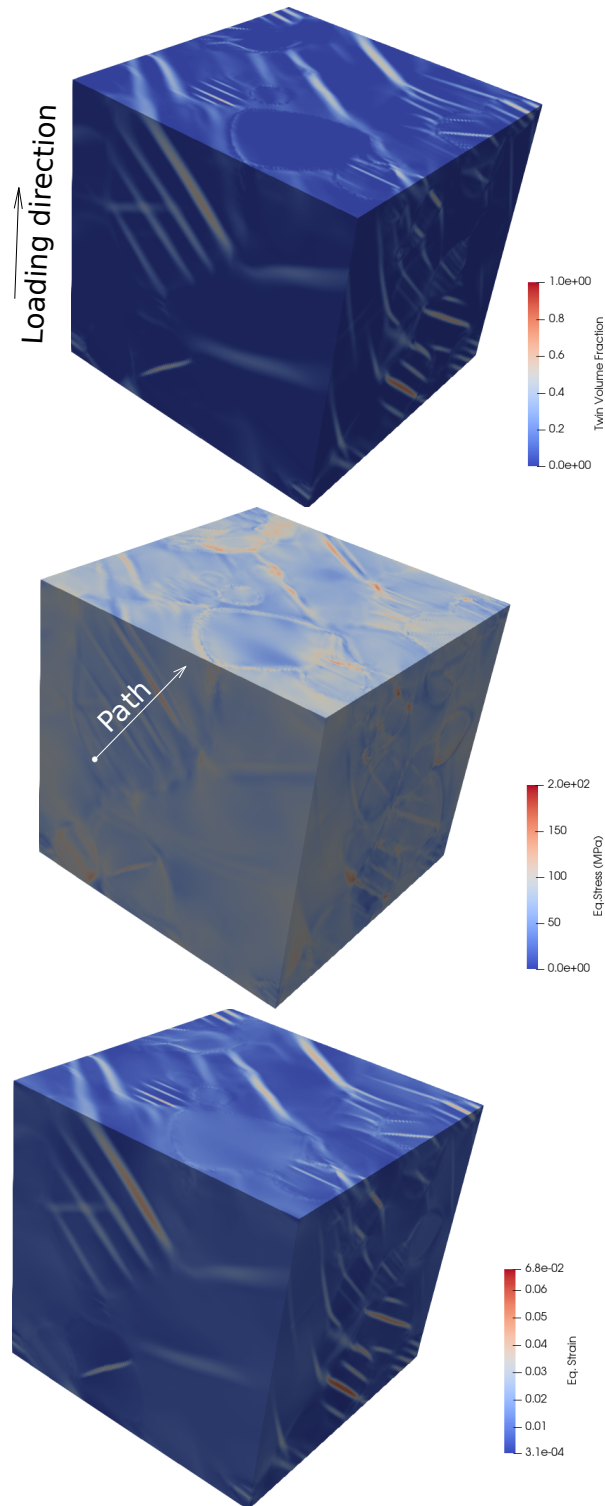


**Figure 4:** (a) Twin volume fraction, (b) equivalent stress and (c) equivalent strain obtained at the end of a uniaxial compression test.

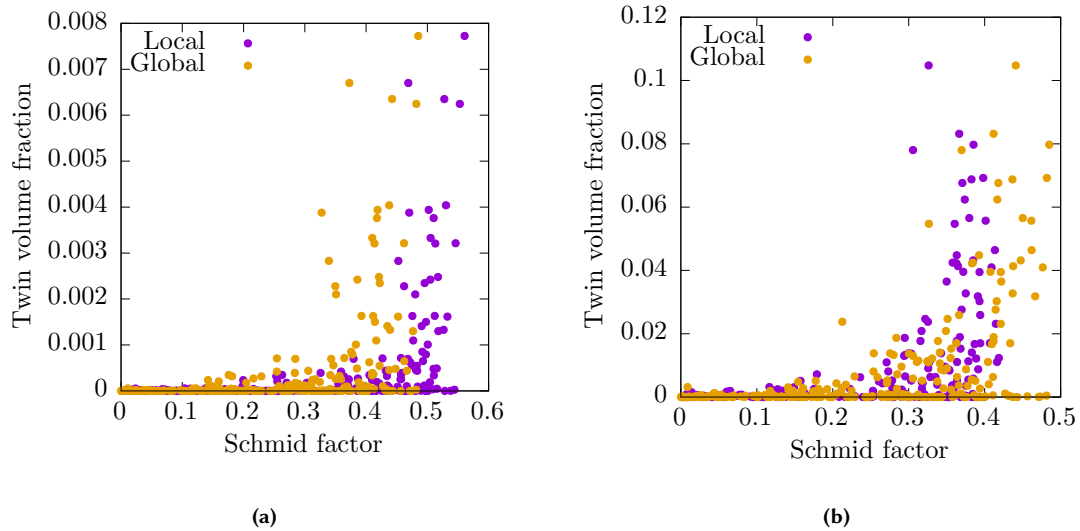


**Figure 5:** (a) Twin volume fraction as a function of the local and global Schmid factors calculated after yielding under uniaxial compression (i.e. -0.16%, left). (b) Twin volume fraction as a function of the local and global Schmid factors calculated at the end of a uniaxial compression test (i.e. -0.5%, right).

Louca et al. (2021) observed that, immediately after yielding, the tangential stress within a twin is in average higher than that of the corresponding parent grain. According to numerical results (see Figure 8), this aspect is underestimated by the present model. The possible reason for such discrepancies might be the fact that the development of plastic strains is not affected by twin boundaries. Indeed, while twin boundaries may limit dislocation motion, their contribution to strain hardening is not considered here. Also, with further deformation under compression, Louca et al. (2021) found that large twins have either similar or lower tangential stresses than their parents. This effect, which is attributed to the opposition of surrounding grains to the accumulation of shear deformation within twinned domains, is correctly reproduced by the proposed model. Indeed, as shown in Figure 8, for large twins, the tangential stresses are significantly relaxed compared to those of the corresponding parent grains at the end of the compression test.

### 3.4.2 Uniaxial compression and tension

The numerical and experimental stress-strain curves obtained for the compression-tension loading path are shown in Figure 9. The deformation behavior under compression is correctly reproduced by the model. Specifically, experimental results indicate a strong Bauschinger effect since yielding occurs almost immediately after load reversal (around -53 MPa). According to the calculated deformation mode activities (see Figure 9), yielding after load reversal is the consequence of both the reactivation of basal slip systems and detwinning. The reactivation of basal systems is made possible thanks to the internal stresses generated during deformation under uniaxial compression. However, the internal stresses are not high enough to reactivate prismatic slip systems. Also, the activity of twinning systems tends toward zero when the axial load is reversed toward tension, which indicates that full detwinning has occurred.

Although basal and prismatic slip systems contribute to plastic deformation under uniaxial tension, the axial stress is overestimated by the proposed model. This poor description of the behavior under tension is likely due to the description of hardening, which relies on a purely isotropic formulation. A more realistic description of the behavior under tension would require considering kinematic hardening.

The basal pole figures obtained from numerical simulations are plotted in Figure 10. The alignment of basal poles from the normal direction toward the rolling direction at the end of the compression stage, which has been observed by Louca et al. (2021), is correctly depicted by the present model. Also, as a consequence of detwinning, basal poles are rotated back toward the normal direction of the specimen at the end of the tension stage.

## 4 Conclusions

A crystal plasticity-based constitutive model for simulating formation of twins in metallic polycrystals is developed. To include the contribution of twinning, each material point is treated as a composite material consisting of a parent constituent and multiple twin variants. The twin volume fractions and their spatial gradients are treated as external state variables to account for the contribution of twin boundaries to free energy. The resulting constitutive model is therefore non-local since the evolution of the twin volume

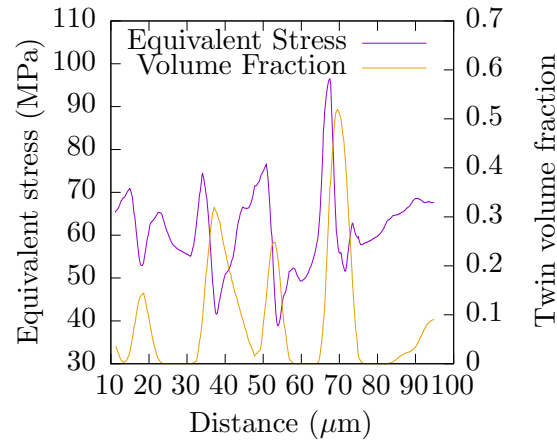


**Figure 6:** Distribution of the twin volume fraction and von Mises equivalent stress along a line path within a twinned grain. The line path is shown in Figure 4.

fraction depends on the state of neighboring material points.

The proposed set of constitutive relations has been implemented in a spectral solver to model the behavior of a AZ31 magnesium alloy. For the investigated loading conditions, the mechanical behavior is mostly controlled by the competition between crystallographic slip and twinning. Specifically, the initial yielding during uniaxial compression coincides with the activation of basal slip systems while the transition toward the plastic regime is attributed to twinning. When the loading direction is reversed toward tension, yielding occurs almost immediately after load reversal because of the joint contributions of detwinning and basal slip. Also, according to the numerical results, the development of texture and internal stresses is consistent with the experimental observations of the literature. Specifically, the proposed model naturally replicates the lenticular shape of twin domains.

Future work should focus on the role of twin boundaries on strain hardening. Indeed, while experimental studies indicate that twin boundaries contribute to strain hardening (Basinski, Z.S. et al. 1997), the impact of twin boundaries on the resistance to dislocation motion has been ignored in the present work. The coupling between slip and twinning deformation modes should therefore be considered for future developments.

## References

- Abdolvand, H., M. R. Daymond, and C. Mareau (2011). "Incorporation of twinning into a crystal plasticity finite element model: Evolution of lattice strains and texture in Zircaloy-2". *International Journal of Plasticity* 27.11, pp. 1721–1738. DOI: [10.1016/j.ijplas.2011.04.005](https://doi.org/10.1016/j.ijplas.2011.04.005). URL: <https://www.sciencedirect.com/science/article/pii/S0749641911000544>
- Abdolvand, H., M. Majkut, J. Oddershede, S. Schmidt, U. Lienert, B. J. Diak, P. J. Withers, and M. R. Daymond (2015). "On the deformation twinning of Mg AZ31B: A three-dimensional synchrotron X-ray diffraction experiment and crystal plasticity finite element model". *International Journal of Plasticity* 70, pp. 77–97. DOI: [10.1016/j.ijplas.2015.03.001](https://doi.org/10.1016/j.ijplas.2015.03.001). URL: <https://www.sciencedirect.com/science/article/pii/S0749641915000443>
- Agnew, S., D. Brown, and C. Tomé (2006). "Validating a polycrystal model for the elastoplastic response of magnesium alloy AZ31 using in situ neutron diffraction". *Acta Materialia* 54.18, pp. 4841–4852. DOI: [10.1016/j.actamat.2006.06.020](https://doi.org/10.1016/j.actamat.2006.06.020). URL: <https://www.sciencedirect.com/science/article/pii/S1359645406004502>
- Ardeljan, M., I. J. Beyerlein, B. A. McWilliams, and M. Knezevic (2016). "Strain rate and temperature sensitive multi-level crystal plasticity model for large plastic deformation behavior: Application to AZ31 magnesium alloy". *International Journal of Plasticity* 83, pp. 90–109. DOI: [10.1016/j.ijplas.2016.04.005](https://doi.org/10.1016/j.ijplas.2016.04.005). URL: <https://www.sciencedirect.com/science/article/pii/S0749641916300481>
- Ardeljan, M., R. J. McCabe, I. J. Beyerlein, and M. Knezevic (2015). "Explicit incorporation of deformation twins into crystal plasticity finite element models". English. *Computer Methods in Applied Mechanics and Engineering* 295.C, pp. 396–413. DOI: [10.1016/j.cma.2015.07.003](https://doi.org/10.1016/j.cma.2015.07.003)
- Arul Kumar, M., B. Clausen, L. Capolungo, R. J. McCabe, W. Liu, J. Z. Tischler, and C. N. Tomé (2018). "Deformation twinning and grain partitioning in a hexagonal close-packed magnesium alloy". *Nature Communications* 9, pp. 1–8. DOI: [10.1038/s41467-018-07028-w](https://doi.org/10.1038/s41467-018-07028-w)

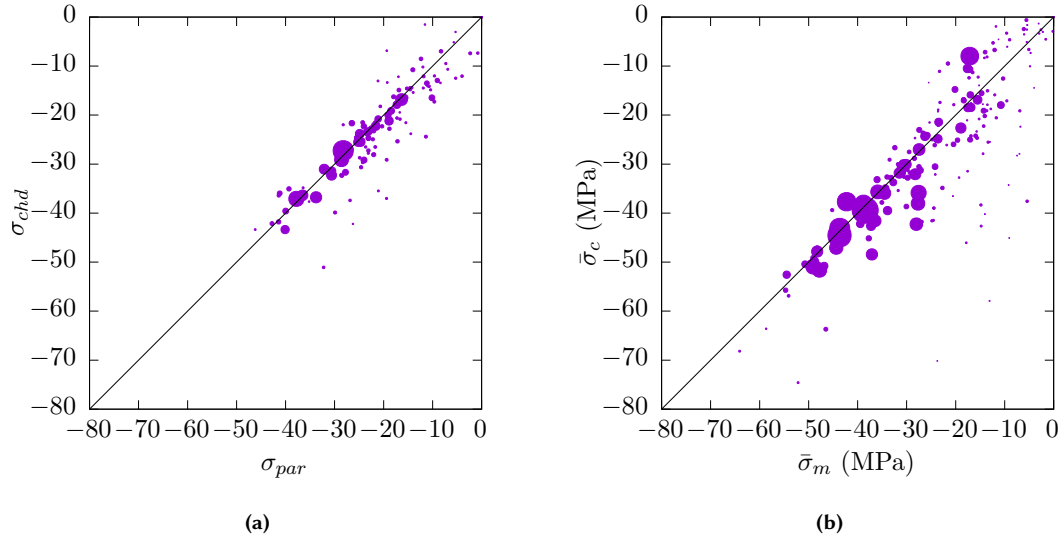


**Figure 7:** Average normal stress exerted by the child grain  $\bar{\sigma}^c$  on the twin habit plane as a function of that of the corresponding parent grain  $\bar{\sigma}^m$ . Normal stresses have been evaluated after (a) yielding under uniaxial compression (i.e. -0.16%) and (b) at the end of the uniaxial compression test (i.e. -0.5%). The size of each dot is proportional to the equivalent spherical radius of the child grain.

- Aydiner, C., J. Bernier, B. Clausen, U. Lienert, C. Tomé, and D. Brown (July 2009). “Evolution of stress in individual grains and twins in a magnesium alloy aggregate”. *Phys. Rev. B* 80 (2), p. 024113. DOI: [10.1103/PhysRevB.80.024113](https://doi.org/10.1103/PhysRevB.80.024113). URL: <https://link.aps.org/doi/10.1103/PhysRevB.80.024113>
- Basinski, Z.S., Szczerba, M.S., Niewczas, M., Embury, J.D., and Basinski, S.J. (1997). “The transformation of slip dislocations during twinning of copper-aluminum alloy crystals”. *Rev. Met. Paris* 94.9, pp. 1037–1044. DOI: [10.1051/metal/199794091037](https://doi.org/10.1051/metal/199794091037). URL: <https://doi.org/10.1051/metal/199794091037>
- Bieler, T., L. Wang, A. Beaudoin, P. Kenesei, and U. Lienert (2014). “In Situ Characterization of Twin Nucleation in Pure Ti Using 3D-XRD”. *Metall Mater Trans A* 45, pp. 109–122. DOI: [10.1007/s11661-013-2082-3](https://doi.org/10.1007/s11661-013-2082-3). URL: <https://doi.org/10.1007/s11661-013-2082-3>
- Brown, D., S. Agnew, M. Bourke, T. Holden, S. Vogel, and C. Tomé (2005). “Internal strain and texture evolution during deformation twinning in magnesium”. *Materials Science and Engineering: A* 399.1. Measurement and Interpretation of Internal/Residual Stresses, pp. 1–12. DOI: [10.1016/j.msea.2005.02.016](https://doi.org/10.1016/j.msea.2005.02.016). URL: <https://www.sciencedirect.com/science/article/pii/S0921509305001541>
- Cermelli, P. and M. Gurtin (2002). “Geometrically necessary dislocations in viscoplastic single crystals and bicrystals undergoing small deformations”. *International Journal of Solids and Structures* 39, pp. 6281–6309
- Chang, Y. and D. M. Kochmann (2015). “A variational constitutive model for slip-twinning interactions in hcp metals: Application to single- and polycrystalline magnesium”. *International Journal of Plasticity* 73. Special Issue on Constitutive Modeling from Micro-Scale to Continuum in Honor of Prof. Frédéric Barlat, pp. 39–61. DOI: [10.1016/j.ijplas.2015.03.008](https://doi.org/10.1016/j.ijplas.2015.03.008). URL: <https://www.sciencedirect.com/science/article/pii/S0749641915000637>
- Cheng, J. and S. Ghosh (2015). “A crystal plasticity FE model for deformation with twin nucleation in magnesium alloys”. *International Journal of Plasticity* 67, pp. 148–170. DOI: [10.1016/j.ijplas.2014.10.005](https://doi.org/10.1016/j.ijplas.2014.10.005). URL: <https://www.sciencedirect.com/science/article/pii/S0749641914001995>
- Cheng, J. and S. Ghosh (2017). “Crystal plasticity finite element modeling of discrete twin evolution in polycrystalline magnesium”. English. *Journal of the Mechanics and Physics of Solids* 99.C, pp. 512–538. DOI: [10.1016/j.jmps.2016.12.008](https://doi.org/10.1016/j.jmps.2016.12.008)
- Cherkaoui, M. (2003). “Constitutive equations for twinning and slip in low-stacking-fault-energy metals: a crystal plasticity-type model for moderate strains”. *Philosophical Magazine* 83.31–34, pp. 3945–3958. DOI: [10.1080/14786430310001603355](https://doi.org/10.1080/14786430310001603355). eprint: <https://doi.org/10.1080/14786430310001603355>. URL: <https://doi.org/10.1080/14786430310001603355>
- Clausen, B., C. Tomé, D. Brown, and S. Agnew (2008). “Reorientation and stress relaxation due to twinning: Modeling and experimental characterization for Mg”. *Acta Materialia* 56.11, pp. 2456–2468. DOI: [10.1016/j.actamat.2008.01.057](https://doi.org/10.1016/j.actamat.2008.01.057). URL: <https://www.sciencedirect.com/science/article/pii/S1359645408000724>
- Clayton, J. and J. Knap (2011). “A phase field model of deformation twinning: Nonlinear theory and numerical simulations”. *Physica D: Nonlinear Phenomena* 240.9, pp. 841–858. DOI: [10.1016/j.physd.2010.12.012](https://doi.org/10.1016/j.physd.2010.12.012). URL: <https://www.sciencedirect.com/science/article/pii/S0167278910003623>

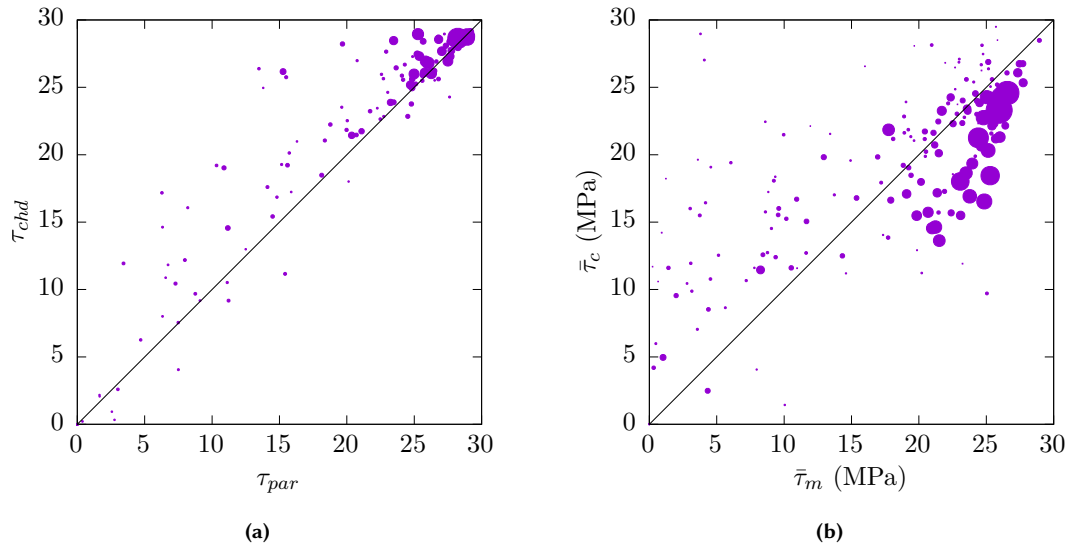


**Figure 8:** Average tangential stress exerted by the child grain  $\bar{\tau}^c$  on the twin habit plane along the twinning direction as a function of that of the corresponding parent grain  $\bar{\tau}^m$ . Tangential stresses have been evaluated (a) after yielding under uniaxial compression (i.e. -0.16%) and (b) at the end of the uniaxial compression test (i.e. -0.5%). The size of each dot is proportional to the equivalent spherical radius of the child grain.

- Eisenlohr, P., M. Diehl, R. Lebensohn, and F. Roters (2013). “A spectral method solution to crystal elasto-viscoplasticity at finite strains”. *International Journal of Plasticity* 46. Microstructure-based Models of Plastic Deformation, pp. 37–53. DOI: [10.1016/j.ijplas.2012.09.012](https://doi.org/10.1016/j.ijplas.2012.09.012). URL: <https://www.sciencedirect.com/science/article/pii/S0749641912001428>
- Frémond, M. and B. Nedjar (1996). “Damage, gradient of damage and principle of virtual power”. *International Journal of Solids and Structures* 33.8, pp. 1083–1103. DOI: [10.1016/0020-7683\(95\)00074-7](https://doi.org/10.1016/0020-7683(95)00074-7). URL: <https://www.sciencedirect.com/science/article/pii/0020768395000747>
- Grilli, N., A. C. Cocks, and E. Tarleton (2020). “A phase field model for the growth and characteristic thickness of deformation-induced twins”. *Journal of the Mechanics and Physics of Solids* 143, p. 104061. DOI: [10.1016/j.jmps.2020.104061](https://doi.org/10.1016/j.jmps.2020.104061). URL: <https://www.sciencedirect.com/science/article/pii/S0022509620302957>
- Guo, Y., H. Abdolvand, T. Britton, and A. Wilkinson (2017). “Growth of {1122} twins in titanium: A combined experimental and modelling investigation of the local state of deformation”. *Acta Materialia* 126, pp. 221–235. DOI: [10.1016/j.actamat.2016.12.066](https://doi.org/10.1016/j.actamat.2016.12.066). URL: <https://www.sciencedirect.com/science/article/pii/S135964541631014X>
- Jiang, L., J. Jonas, R. Mishra, A. Luo, A. Sachdev, and S. Godet (2007). “Twinning and texture development in two Mg alloys subjected to loading along three different strain paths”. *Acta Materialia* 55.11, pp. 3899–3910. DOI: [10.1016/j.actamat.2007.03.006](https://doi.org/10.1016/j.actamat.2007.03.006). URL: <https://www.sciencedirect.com/science/article/pii/S1359645407001899>
- Juan, P.-A., S. Berbenni, M. Barnett, C. Tomé, and L. Capolungo (2014). “A double inclusion homogenization scheme for polycrystals with hierarchical topologies: application to twinning in Mg alloys”. *International Journal of Plasticity* 60, pp. 182–196. DOI: [10.1016/j.ijplas.2014.04.001](https://doi.org/10.1016/j.ijplas.2014.04.001). URL: <https://www.sciencedirect.com/science/article/pii/S0749641914000722>
- Kalidindi, S. R. (2001). “Modeling anisotropic strain hardening and deformation textures in low stacking fault energy fcc metals”. *International Journal of Plasticity* 17.6, pp. 837–860. DOI: [10.1016/S0749-6419\(0\)00071-1](https://doi.org/10.1016/S0749-6419(0)00071-1). URL: <https://www.sciencedirect.com/science/article/pii/S0749641900000711>
- Kondo, R., Y. Tadano, and K. Shizawa (2014). “A phase-field model of twinning and detwinning coupled with dislocation-based crystal plasticity for HCP metals”. *Computational Materials Science* 95, pp. 672–683. DOI: [10.1016/j.commatsci.2014.08.034](https://doi.org/10.1016/j.commatsci.2014.08.034). URL: <https://www.sciencedirect.com/science/article/pii/S092702561400576X>
- Liu, C., P. Shanthraj, M. Diehl, F. Roters, S. Dong, J. Dong, W. Ding, and D. Raabe (2018). “An integrated crystal plasticity–phase field model for spatially resolved twin nucleation, propagation, and growth in hexagonal materials”. *International Journal of Plasticity* 106, pp. 203–227. DOI: [10.1016/j.ijplas.2018.03.009](https://doi.org/10.1016/j.ijplas.2018.03.009). URL: <https://www.sciencedirect.com/science/article/pii/S0749641917307209>
- Louca, K., H. Abdolvand, C. Mareau, M. Majkut, and J. Wright (2021). “Formation and annihilation of stressed deformation twins in magnesium”. *Communications Materials* 2. DOI: [10.1038/s43246-020-00105-y](https://doi.org/10.1038/s43246-020-00105-y). URL: <https://doi.org/10.1038/s43246-020-00105-y>
- Mareau, C. and M. R. Daymond (2011). “Comparison of experimentally determined texture development in Zircaloy-2 with predictions from a rate-dependent polycrystalline model”. *Materials Science and*



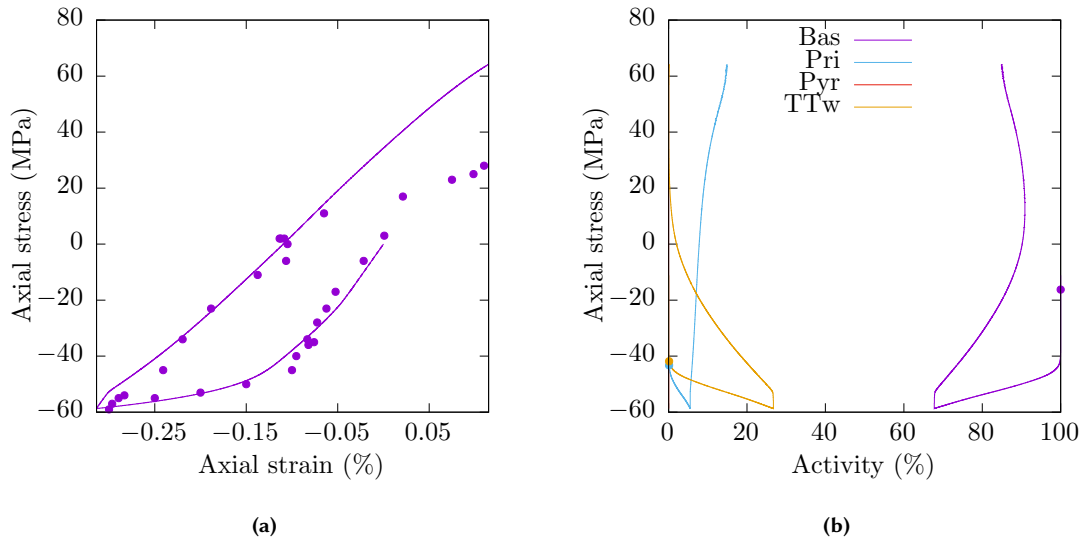


**Figure 9:** (a) Experimental and numerical stress-strain curves obtained for a uniaxial compression and tension test along the rolling direction. (b) Relative activities of the different inelastic deformation modes. The first activation of a given type of slip or twinning system is represented with a dot.

*Engineering: A* 528.29, pp. 8676–8686. DOI: [10.1016/j.msea.2011.08.040](https://doi.org/10.1016/j.msea.2011.08.040). URL: <https://www.sciencedirect.com/science/article/pii/S0921509311009257>

Mareau, C. and M. R. Daymond (2016). “Micromechanical modelling of twinning in polycrystalline materials: Application to magnesium”. *International Journal of Plasticity* 85, pp. 156–171. DOI: [10.1016/j.ijplas.2016.07.007](https://doi.org/10.1016/j.ijplas.2016.07.007). URL: <https://www.sciencedirect.com/science/article/pii/S0749641916301140>

Moulinec, H. and P. Suquet (1998). “A numerical method for computing the overall response of nonlinear composites with complex microstructure”. *Computer Methods in Applied Mechanics and Engineering* 157.1, pp. 69–94. DOI: [10.1016/S0045-7825\(97\)00218-1](https://doi.org/10.1016/S0045-7825(97)00218-1). URL: <https://www.sciencedirect.com/science/article/pii/S0045782597002181>

Nervo, L., A. King, A. Fitzner, W. Ludwig, and M. Preuss (2016). “A study of deformation twinning in a titanium alloy by X-ray diffraction contrast tomography”. *Acta Materialia* 105, pp. 417–428. DOI: [10.1016/j.actamat.2015.12.032](https://doi.org/10.1016/j.actamat.2015.12.032). URL: <https://www.sciencedirect.com/science/article/pii/S1359645415301385>

Nguyen, Q.-S. (2000). *Stability and Nonlinear Solid Mechanics*. Chichester: John Wiley & Sons, LTD

Nguyen, Q.-S. (2015). “Some remarks on standard gradient models and gradient plasticity”. *Mathematics and Mechanics of Solids* 20.6, pp. 760–769. DOI: [10.1177/1081286514551499](https://doi.org/10.1177/1081286514551499). eprint: <https://doi.org/10.1177/1081286514551499>. URL: <https://doi.org/10.1177/1081286514551499>

Paramatmuni, C. and F. P. Dunne (2020). “Effect of twin crystallographic orientation on deformation and growth in Mg alloy AZ31”. *International Journal of Plasticity* 135, p. 102775. DOI: [10.1016/j.ijplas.2020.102775](https://doi.org/10.1016/j.ijplas.2020.102775). URL: <https://www.sciencedirect.com/science/article/pii/S0749641919307533>

Paramatmuni, C., Y. Guo, P. J. Withers, and F. P. Dunne (2021). “A three-dimensional mechanistic study of the drivers of classical twin nucleation and variant selection in Mg alloys : a mesoscale modelling and experimental study”. *International Journal of Plasticity*, p. 103027. DOI: <https://doi.org/10.1016/j.ijplas.2021.103027>. URL: <https://www.sciencedirect.com/science/article/pii/S0749641921001029>

Paramatmuni, C. and A. K. Kanjarla (2019). “A crystal plasticity FFT based study of deformation twinning, anisotropy and micromechanics in HCP materials: Application to AZ31 alloy”. *International Journal of Plasticity* 113, pp. 269–290. DOI: [10.1016/j.ijplas.2018.10.007](https://doi.org/10.1016/j.ijplas.2018.10.007). URL: <https://www.sciencedirect.com/science/article/pii/S0749641918303851>

Pei, Z., X. Zhang, T. Hickel, M. Friák, S. Sandlöbes, B. Dutta, and J. Neugebauer (2017). “Atomic structures of twin boundaries in hexagonal close-packed metallic crystals with particular focus on Mg”. *npj Computational Materials* 3. DOI: [10.1038/s41524-017-0010-6](https://doi.org/10.1038/s41524-017-0010-6). URL: <https://doi.org/10.1038/s41524-017-0010-6>

Poulsen, H. F., S. F. Nielsen, E. M. Lauridsen, S. Schmidt, R. M. Suter, U. Lienert, L. Margulies, T. Lorentzen, and D. Juul Jensen (Dec. 2001). “Three-dimensional maps of grain boundaries and the stress state of individual grains in polycrystals and powders”. *Journal of Applied Crystallography* 34.6, pp. 751–756. DOI: [10.1107/S0021889801014273](https://doi.org/10.1107/S0021889801014273). URL: <https://doi.org/10.1107/S0021889801014273>

Proust, G., C. Tomé, and G. Kaschner (2007). “Modeling texture, twinning and hardening evolution during deformation of hexagonal materials”. *Acta Materialia* 55.6, pp. 2137–2148. DOI: [10.1016/j.actamat.2006.11.017](https://doi.org/10.1016/j.actamat.2006.11.017). URL: <https://www.sciencedirect.com/science/article/pii/S1359645406008251>



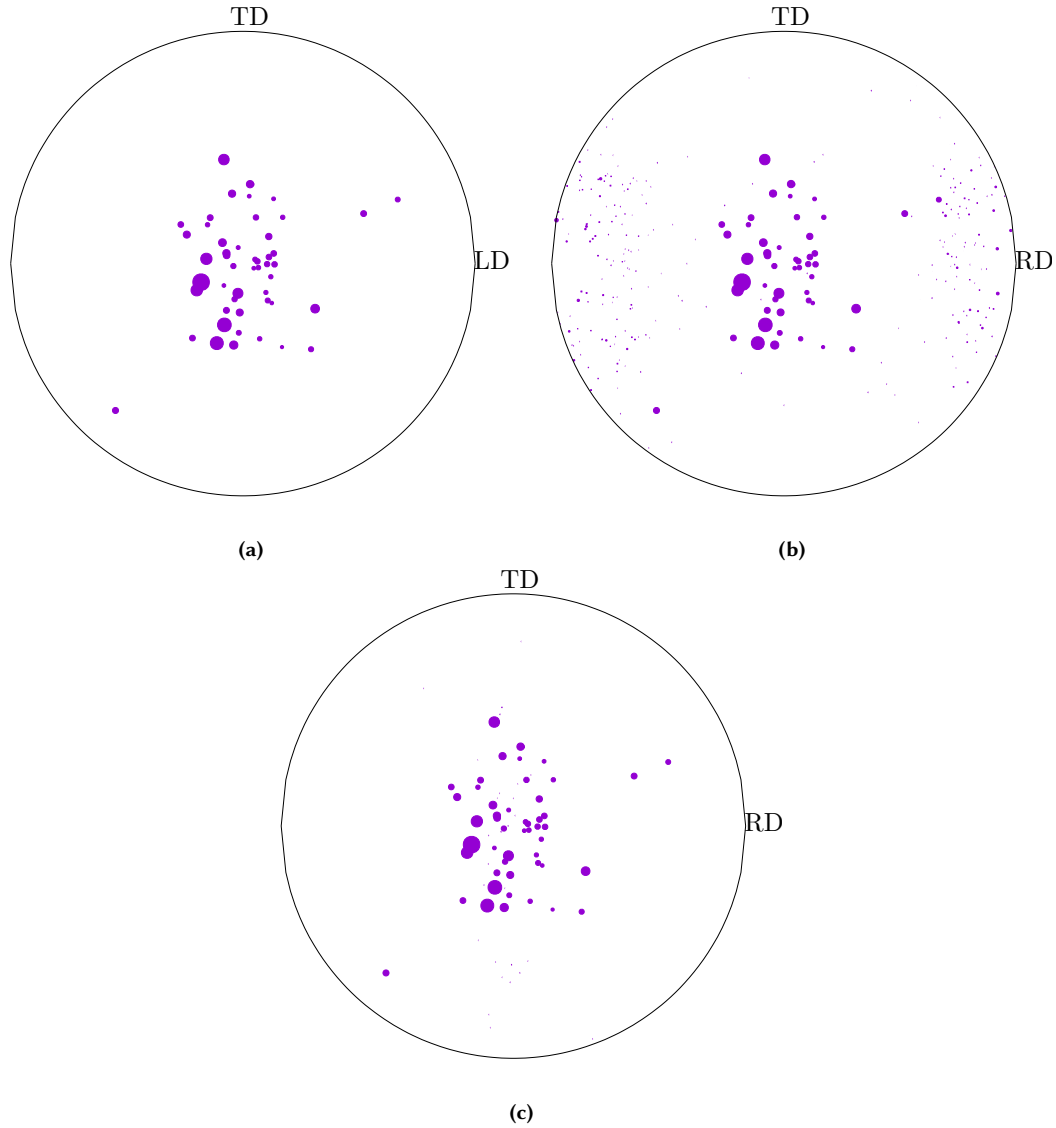


**Figure 10:** (a) Initial, (b) intermediate and (c) final basal pole figures obtained during a compression and tension test. The intermediate and final pole figures correspond respectively to the end of the compression stage (i.e.  $-0.31\%$ ) and the end of the tension stage (i.e.  $0.13\%$ ). The size of each dot is proportional to the equivalent spherical radius of the grain.

- Proust, G., C. Tomé, A. Jain, and S. R. Agnew (2009). “Modeling the effect of twinning and detwinning during strain-path changes of magnesium alloy AZ31”. *International Journal of Plasticity* 25.5, pp. 861–880. DOI: [10.1016/j.ijplas.2008.05.005](https://doi.org/10.1016/j.ijplas.2008.05.005). URL: <https://www.sciencedirect.com/science/article/pii/S074964190800079X>
- Simmons, G. and H. Wang (1971). *Single Crystal Elastic Constants and Calculated Aggregate Properties: A Handbook*. Cambridge, MA: The MIT Press
- Staroselsky, A. and L. Anand (2003). “A constitutive model for hcp materials deforming by slip and twinning: application to magnesium alloy AZ31B”. *International Journal of Plasticity* 19.10, pp. 1843–1864. DOI: [10.1016/S0749-6419\(03\)00039-1](https://doi.org/10.1016/S0749-6419(03)00039-1). URL: <https://www.sciencedirect.com/science/article/pii/S0749641903000391>
- Wang, H., P. Wu, S. Kurukuri, M. J. Worswick, Y. Peng, D. Tang, and D. Li (2018). “Strain rate sensitivities of deformation mechanisms in magnesium alloys”. *International Journal of Plasticity* 107, pp. 207–222. DOI: [10.1016/j.ijplas.2018.04.005](https://doi.org/10.1016/j.ijplas.2018.04.005). URL: <https://www.sciencedirect.com/science/article/pii/S0749641917306459>
- Wu, L., S. Agnew, D. Brown, G. Stoica, B. Clausen, A. Jain, D. Fielden, and P. Liaw (2008). “Internal stress relaxation and load redistribution during the twinning–detwinning-dominated cyclic deformation of a wrought magnesium alloy, ZK60A”. *Acta Materialia* 56.14, pp. 3699–3707. DOI: [10.1016/j.actamat.2008.04.006](https://doi.org/10.1016/j.actamat.2008.04.006). URL: <https://www.sciencedirect.com/science/article/pii/S1359645408002577>
- Xu, F., R. Holt, and M. R. Daymond (2008). “Modeling lattice strain evolution during uniaxial deformation of textured Zircaloy-2”. *Acta Materialia* 56.14, pp. 3672–3687. DOI: [10.1016/j.actamat.2008.04.019](https://doi.org/10.1016/j.actamat.2008.04.019). URL: <https://www.sciencedirect.com/science/article/pii/S1359645408002553>

- Xu, F., R. Holt, and M. R. Daymond (2009). “Modeling texture evolution during uni-axial deformation of Zircaloy-2”. *Journal of Nuclear Materials* 394.1, pp. 9–19. DOI: [10.1016/j.jnucmat.2009.07.006](https://doi.org/10.1016/j.jnucmat.2009.07.006). URL: <https://www.sciencedirect.com/science/article/pii/S0022311509007168>
- Xu, F., R. Holt, M. R. Daymond, R. Rogge, and E. Oliver (2008). “Development of internal strains in textured Zircaloy-2 during uni-axial deformation”. *Materials Science and Engineering: A* 488.1, pp. 172–185. DOI: [10.1016/j.msea.2007.11.018](https://doi.org/10.1016/j.msea.2007.11.018). URL: <https://www.sciencedirect.com/science/article/pii/S0921509307018266>
- Yang, H. J., S. M. Yin, C. X. Huang, Z. F. Zhang, S. D. Wu, S. X. Li, and Y. D. Liu (2008). “EBSD Study on Deformation Twinning in AZ31 Magnesium Alloy During Quasi-in-Situ Compression”. *Advanced Engineering Materials* 10.10, pp. 955–960. DOI: [10.1002/adem.200800111](https://doi.org/10.1002/adem.200800111). eprint: <https://onlinelibrary.wiley.com/doi/pdf/10.1002/adem.200800111>. URL: <https://onlinelibrary.wiley.com/doi/abs/10.1002/adem.200800111>

**Open Access** This article is licensed under a Creative Commons Attribution 4.0 International License, which permits use, sharing, adaptation, distribution and reproduction in any medium or format, as long as you give appropriate credit to the original author(s) and the source, provide a link to the Creative Commons license, and indicate if changes were made. The images or other third party material in this article are included in the article’s Creative Commons license, unless indicated otherwise in a credit line to the material. If material is not included in the article’s Creative Commons license and your intended use is not permitted by statutory regulation or exceeds the permitted use, you will need to obtain permission directly from the copyright holder. To view a full copy of this license, visit <http://creativecommons.org/licenses/by/4.0/>.